

# Supplementary material to manuscript "High-resolution modelling of early contrail evolution from hydrogen-powered aircraft"

Annemarie Lottermoser and Simon Unterstrasser

Deutsches Zentrum für Luft- und Raumfahrt, Institut für Physik der Atmosphäre, Oberpfaffenhofen, Germany

**Correspondence:** Annemarie Lottermoser (annemarie.lottermoser@dlr.de)

## S1 Temporal and spatial evolution of temperature and humidity during the vortex phase

Figure S1 illustrates the evolution of ice relative humidity (a) and temperature difference (b), where the background temperature profile has been subtracted. Within the wake vortices, the ice relative humidity remains close to saturation until the vortices dissipate. This phenomenon results from the sublimation of ice crystals trapped in the primary wake. The sublimation increases the local water vapor concentration, balancing the decrease in  $RH_i$  caused by adiabatic heating. Note that humidity values below 100 % may occur as the sublimation does not instantaneously relax the humidity field to saturation. In the secondary wake,  $RH_i$  also remains near saturation as detrained ice crystals deplete ambient moisture, reducing the environmental supersaturation toward saturation. The presented humidity fields are quite smooth as they are averages along flight direction.

Initially, the temperature perturbation is nearly everywhere close to zero. The centers of the wake vortices feature a pressure drop to compensate for centrifugal forces and can lead to a very localized temperature drop. Due to the prescribed stable stratification, air masses at the original flight altitude have a higher potential temperature than air masses beneath. Hence, the descending primary wake is identified by positive  $\Delta T$  values. A similar consideration explains the negative  $\Delta T$  values after six minutes around  $z = 0$  m. Air masses from the primary wake rise back to the initial altitude and push or contain also air masses from lower altitudes (with lower potential temperature) to  $z = 0$  m leading to  $\Delta T < 0$  K.

## S2 Further information on ice crystal loss parametrization

### S2.1 Evaluation of $z_{\text{atm}}$ and $z_{\text{emit}}$

In the ice crystal loss parametrization, the two length scales  $z_{\text{atm}}$  and  $z_{\text{emit}}$  are implicitly defined. In the original version in U2016 (= Unterstrasser, 2016), the nonlinear equations were solved using a numerical method (classical bisection method). To speed up evaluations and to provide explicit formulations, fit formulae for the two length scales  $z_{\text{atm}}$  and  $z_{\text{emit}}$  were derived as outlined in Sec. (A3) of this study. In order to compare both versions simulation-wise, the length scale values determined with the bisection method and the fit formulae are compared. Moreover, the corresponding survival fractions based on either evaluation method are calculated. The outcomes are provided in Tab. S1. As noted in the main text, applying the analytical

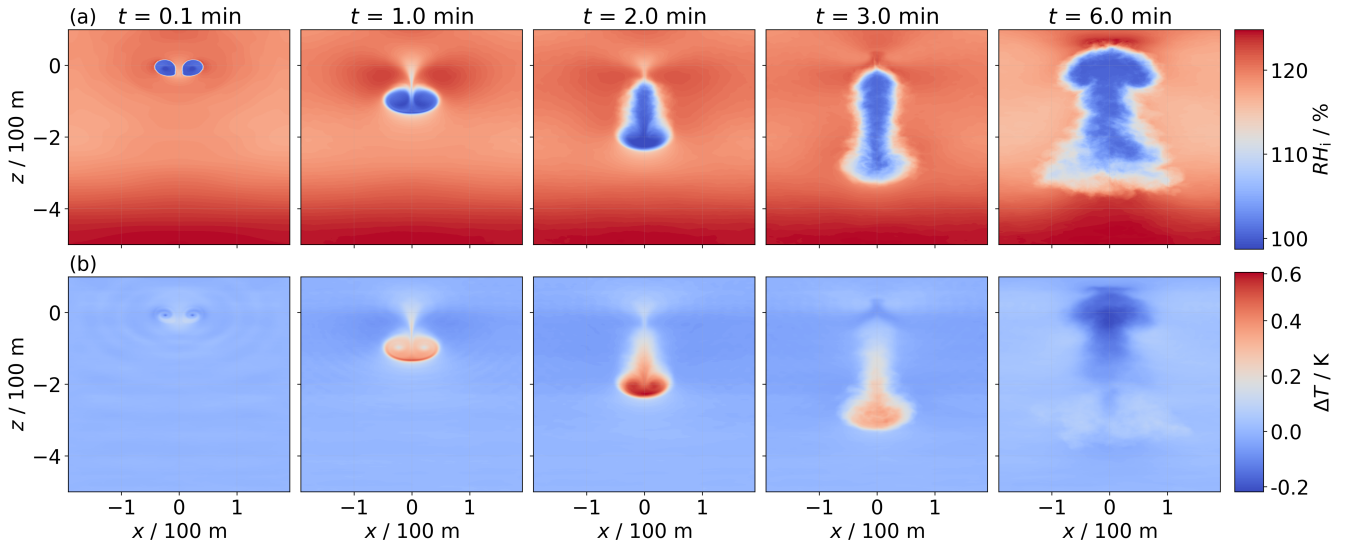


**Figure S1.** Temporal evolution of relative humidity with respect to ice (a) and temperature difference (b) in the  $x, z$ -plane (averaged along flight direction). In (b), the vertical background temperature profile is subtracted to highlight the temperature evolution, particularly within the primary wake. Note that the first column corresponds to 0.1 min, whereas the zeroth time step is shown in the main body of the manuscript. This distinction is made because the thermodynamic fields exhibit almost no visible features at the initial time step. The depicted exemplary simulation is performed for an A350/B777-like aircraft at  $T_{CA} = 217\text{ K}$ ,  $RH_{i,amb} = 120\%$ ,  $N_{BV} = 1.15 \times 10^{-2}\text{ s}^{-1}$ ,  $N_0 = 3.38 \times 10^{12}\text{ m}^{-1}$ ,  $I_0 = 15.0\text{ g m}^{-1}$ , and  $r_{SD} = 3.0$ .

relations to compute the parametrized survival fraction yields no change for 44 % of the data points (rounded to two decimal places, as in Tab. A1), and the maximum deviation observed is 2 %.

## 25 S2.2 Comparison of the original and new ice crystal loss parametrization

The original ice crystal loss parametrization proposed in U2016 has been implemented in several larger-scale contrail models to refine the contrail initialization in those models (Gruber et al., 2018; Bier and Burkhardt, 2022), and applications were restricted to conventional kerosene contrails.

This section presents comparison plots between the original and updated version of the ice crystal loss parametrization. Figure S2 shows scatter plots of  $z_{\Delta}$  (panel (a)) and the parametrized survival fraction  $\hat{f}_{N,s}$  (panel (b)), with the  $x$ -axis representing the original (2016) values and the  $y$ -axis showing the updated (2025) data. The values of  $z_{\Delta}$  are similar across both formulations, although  $z_{\Delta,2025}$  is generally slightly lower. However, differences in  $z_{\Delta}$  should not be over-interpreted as this quantity serves as argument in an arctan-type function (see Eq. (12)) to retrieve the survival fraction. The arctan-type function formulation includes three fit coefficients that change from one to the other version. Hence, panel (b) shows the eventual differences in the parametrized survival fraction from the two versions. Likewise,  $\hat{f}_{N,s}$  exhibits only minor scatter between the two versions.

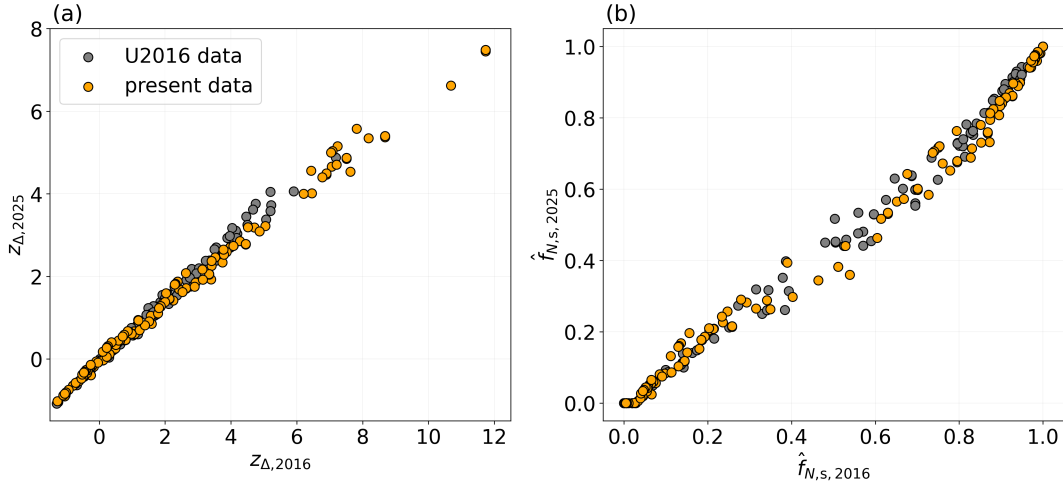


**Figure S2.** Scatter plot comparing the 2016  $z_{\Delta}$  values with the  $z_{\Delta}$  values from the present study (a), and a similar comparison for the parametrized survival fractions (b).

Furthermore, we reproduce plots that were shown in U2016 (Figs. 5, 9, and 10 in that publication). In the new versions of those plots (Figs. S3-S5 in this document), we juxtapose the outcome of the original and the new parametrization. This should demonstrate that the switch to the new formulation has only marginal implications on applications focusing on conventional kerosene contrails.

### S3 Sensitivity analyses: Numerical and physical aspects

In the following, three sensitivity studies are presented. We compare the results of a reference simulation, performed for an A350/B777-like aircraft at  $T_{CA} = 217\text{ K}$ ,  $RH_{i,amb} = 120\%$ ,  $N_{BV} = 1.15 \times 10^{-2} \text{ s}^{-1}$ ,  $N_0 = 3.38 \times 10^{12} \text{ m}^{-3}$ ,  $I_0 = 15.0 \text{ g m}^{-1}$ , and  $r_{SD} = 3.0$  (solid black lines in Fig. S6). These are compared to simulations in which the grid resolution, domain size, and ambient pressure are varied individually.

#### S3.1 Impact of grid resolution

In the reference setup, we employ a horizontal and vertical grid spacing of 1 m. To assess the sensitivity of contrail evolution to mesh resolution, we conduct an additional simulation using a finer resolution of 0.5 m. As shown by the magenta curves in Fig. S6, the higher-resolution simulation results in a relative increase of 7.7 % in total ice mass and a reduction in ice crystal survival fraction from 64.7 % to 62.1 %. Vertical profiles of ice crystal number and mass (not shown) indicate that, in the high-resolution setup, fewer ice crystals are detrained from the vortex system. Instead, a larger fraction remains trapped within the primary wake, where they are more prone to sublimation due to adiabatic heating. The reduced detrainment can be attributed to the way secondary vorticity, generated by baroclinic torque arising from density and pressure gradients between the wake

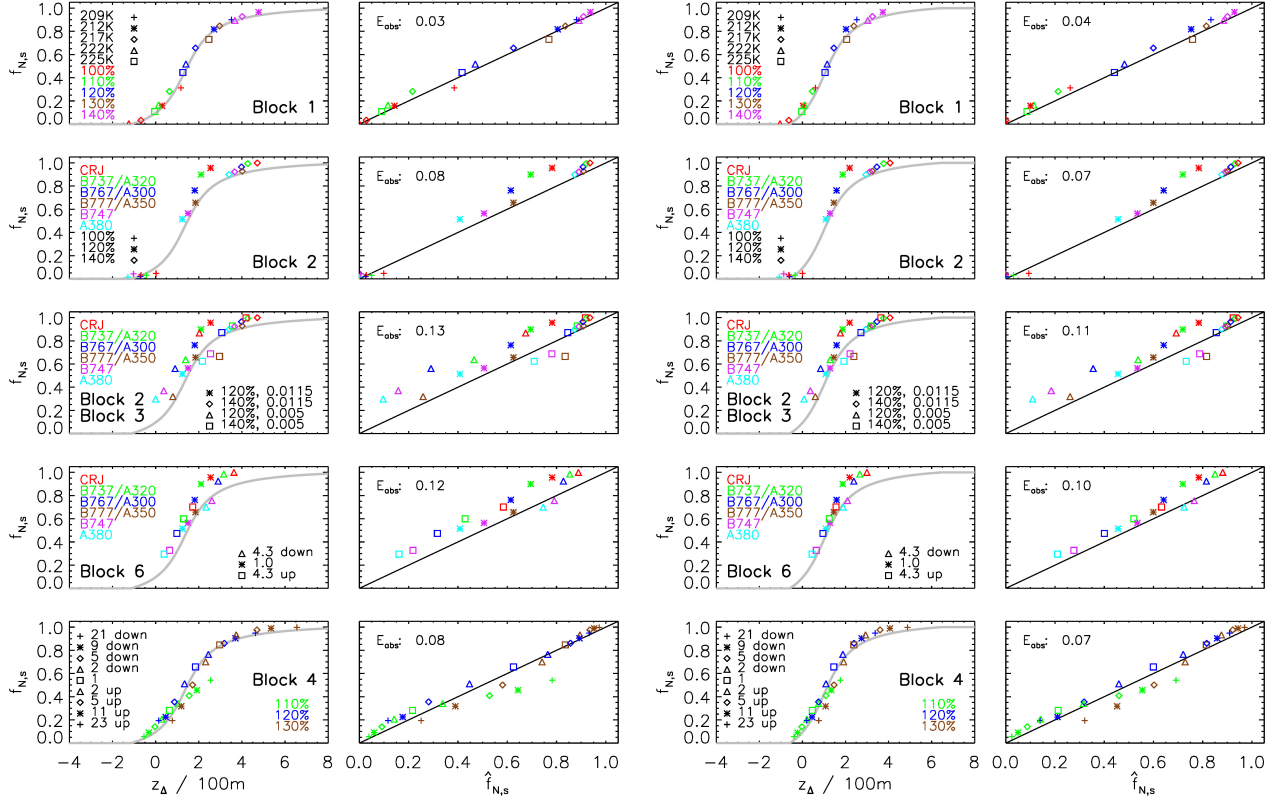


**Figure S3.** Reproduced version of Fig. 5 in U2016. The first two columns show the original plot from U2016. The third and fourth columns use the parametrized survival fractions as obtained from the new parametrization version described in the present study.

Adapted figure caption of U2016:

*Columns 1 and 3: Relationship between simulated survival fraction  $f_{N,s}$  and  $z_{\Delta}$ . The grey curve shows the fit function  $\hat{a}(z_{\Delta})$  as defined in Eq. (12) in the present study.*

*Columns 2 and 4: Relationship between simulated survival fraction  $f_{N,s}$  and approximated survival fraction  $\hat{f}_{N,s}$ . The black line shows the one-to-one line. Each row shows a subset of simulations taken from various simulation blocks defined in Table A2 of U2016. For example, the first row shows simulations of block 1, where  $RH_i$  and  $T_{CA}$  are varied. The legend in the plot provides a list of the symbols and colors, which uniquely defines the simulation parameters of each plotted data point. The root mean square of the absolute error  $\hat{f}_{N,s} - f_{N,s}$  is denoted as  $E_{abs}$  and given for each subset.*

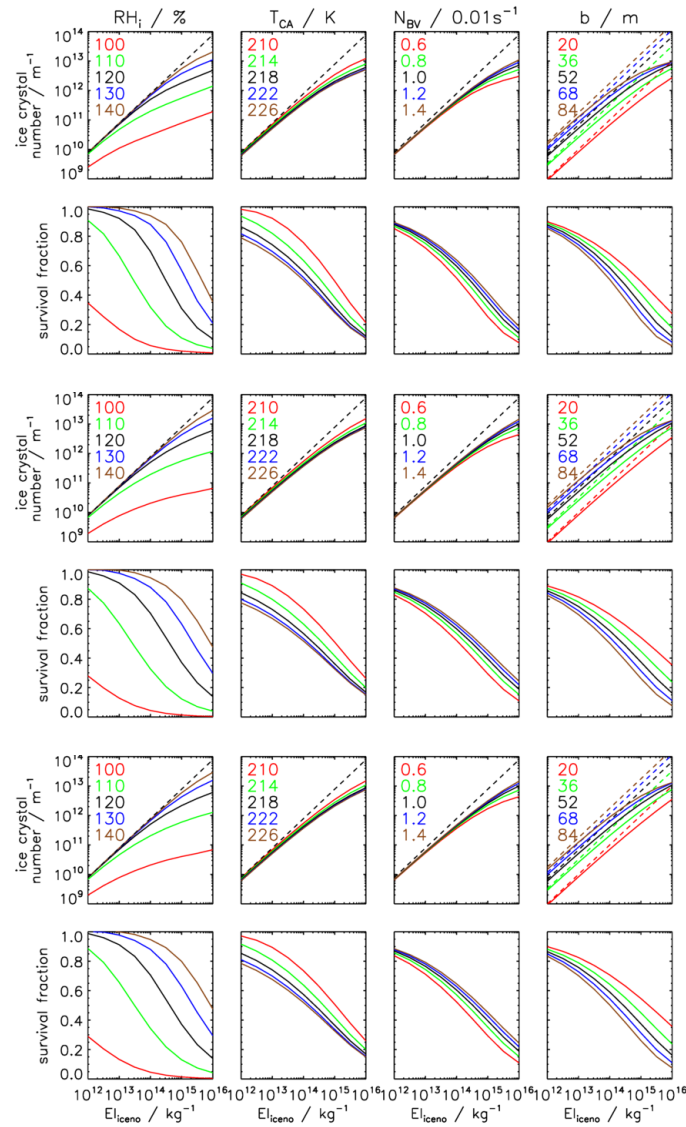


**Figure S4.** Reproduced version of Fig. 9 in U2016. The first two rows show the original plot from U2016. The other rows use the parametrized survival fractions as obtained from the new parametrization version described in the present study evaluating  $z_{\text{atm}}$  and  $z_{\text{emit}}$  either via bisection (rows 3 and 4) or by employing the fit functions (rows 5 and 6).

Adapted figure caption of U2016:

*Sensitivity of ice crystal loss to  $El_{\text{iceno}}$  for various values of  $RH_i$ ,  $T$ ,  $N_{BV}$ , and  $b$  (from left to right). See legend for the color coding. Rows 1, 3, and 5: Ice crystal number per meter of flight path before and after the vortex phase (dashed and solid curves). Note that the initial ice crystal number depends only on  $b$  and  $El_{\text{iceno}}$  (following Eq. (A10) in U2016, which assumes a water vapor emission index of  $1.25 \text{ kg kg}^{-1}$ ). Hence, only one dashed curve is shown in the columns for  $RH_i$ ,  $T$ , and  $N_{BV}$ , respectively. Rows 2, 4, and 6: Survival fraction.*

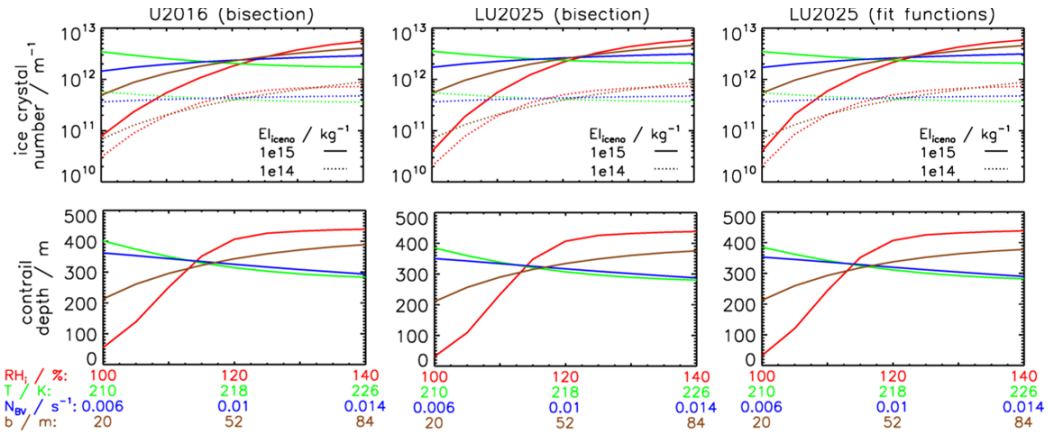


**Figure S5.** Reproduced version of Fig. 10 in U2016. The first column shows the original plot from U2016. The two other columns use the new parametrization version (for both types of  $z_{\text{atm}}$  and  $z_{\text{emit}}$ ).

Adapted figure caption of U2016:

*Ice crystal number per meter of flight path (top) and contrail depth (bottom) after the vortex phase as a function of  $RH_i$ ,  $T$ ,  $N_{BV}$ , or  $b$ .  $EI_{\text{ice}}$  is  $10^{15}$  or  $10^{14} \text{ kg}^{-1}$ . The contrail depth parametrization does not depend on  $EI_{\text{ice}}$ . Note that the parametrization of the contrail depth  $H$  was not updated in the present study. The slightly different results come from the fact that the parametrization of  $H$  uses the parametrized  $f_{N,s}$  value as input. Note that the original plot in U2016 showed an additional panel with ice crystal number concentrations, which is left out here.*

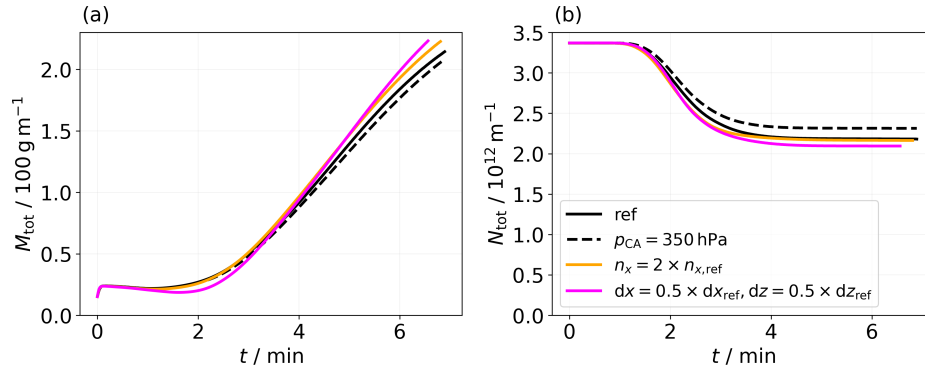


**Figure S6.** Evolution of total ice crystal number (a) and total ice mass (b) for the reference case and three sensitivity simulations, differentiated by color and line style. The dashed black curves represent a simulation conducted at a higher ambient pressure value. The orange curves correspond to a simulation with doubled domain width. The magenta curves show the results from a simulation with a higher mesh resolution in transverse and vertical direction.

and the ambient air (Holzäpfel et al., 2001), develops in the simulation. Although the underlying physical conditions, such as pressure and density gradients, remain unchanged, the finer grid spacing enables a more accurate resolution of these instabilities, potentially altering the dynamics of vortex destabilization. We hypothesize that the improved representation of secondary vorticity results in less disruption of the vortex cores, thereby reducing ice crystal detrainment and increasing sublimation within the primary wake. Alongside this physical explanation of the observed results, we note that background turbulence could likewise influence the detrainment process and contribute to the observed behavior. While the resulting discrepancies in ice crystal number and mass are moderate compared to those induced by variations in the initial ice crystal number, they underscore the relevance of mesh resolution and its potential impact on simulation outcomes. However, in the context of a sensitivity study focused on variations in initial ice crystal number, where ice crystal survival fractions span the full range from 0 to 100 %, we consider deviations in ice crystal survival fraction below 3 % to be minor. Given the substantial computational demands of finer mesh resolutions (roughly eight times higher CPU time) and considering the comparatively minor differences in simulation outcomes, we consider the baseline resolution appropriate for the objectives of this study.

### S3.2 Impact of domain size

The default domain size in the transverse direction is 384 grid boxes, corresponding to 384 m in our reference A350/B777 simulation with a grid spacing of  $dx = 1$  m. In a sensitivity simulation, we increase the domain width from 384 m to 768 m; the results are shown as orange curves in Fig. S6. This modification yields a slight reduction in final ice crystal survival fraction from 64.7 % to 64.2 % and a relative increase of 4.6 % in final ice mass. A plausible explanation is that, in the narrower domain, the descending vortex pairs might interact across the transverse boundaries, damping their descent and thereby enhancing ice crystal survival. Horizontal profiles reveal that, from about two minutes onward, the wider-domain simulation exhibits slightly lower ice crystal number and mass near the outer edges of the vortices, while more ice crystals and ice mass are found in the vortex centers. This supports the hypothesis that transverse interactions across the boundaries in the narrow domain might influence vortex dynamics and particle motion. However, it is equally plausible that the minor deviations in the evolution of ice crystal number and mass reflect variability introduced by background turbulence, as discussed in the previous section. As the wider domain has a negligible effect on the contrail properties, most notably the ice crystal survival fraction, yet significantly increases computational expense, a transverse width of 384 grid boxes is deemed sufficient for our simulations.

### S3.3 Impact of pressure variation

A variation of the ambient pressure value has only minor impact on the evolution of ice crystal mass and number, see black dashed curves in Fig. S6. The pressure at flight altitude of the reference simulation is 231 hPa. We increase the pressure to 350 hPa, keeping all other setup parameters (specifically ambient temperature) unchanged. We observe a slightly reduced final ice mass and a slightly increased number of surviving ice crystals in the higher-pressure case. These differences can be primarily attributed to the pressure dependence of water vapor diffusivity, which appears in the governing equation for ice mass growth (Sölch and Kärcher, 2010). Since diffusivity is inversely proportional to pressure, higher ambient pressure leads to lower diffusivity, thereby reducing the rate of ice crystal growth. Conversely, sublimation is also reduced under higher pressure for the

same reason, leading to a slightly higher survival fraction. An additional, though secondary, factor is the pressure dependence of sedimentation velocity. Increased pressure results in a small reduction in sedimentation velocity. However, for a pressure increase of 120 hPa, the resulting change in sedimentation velocity is on the order of 0.5 %, and is thus considered negligible in this context. Overall, the sensitivity of contrail evolution to ambient pressure variations is weak. The final ice crystal survival fraction changes from 64.7 % to 68.7 %, and the total ice mass differs relatively by 4.0 %. This limited sensitivity is expected: the amount of available atmospheric water vapor, expressed in terms of water vapor concentration  $\rho_{\text{WV,avail}} = (RH_{\text{i,amb}} - 1) \times \rho_{\text{WV,sat,ice}} = (RH_{\text{i,amb}} - 1) \times \frac{e_s(T)}{R_{\text{WV}} T}$ , is primarily temperature-dependent and independent of ambient pressure. Moreover, the adiabatic heating in the descending vortex pair does not depend on ambient pressure.



- Bier, A. and Burkhardt, U.: Impact of Parametrizing Microphysical Processes in the Jet and Vortex Phase on Contrail Cirrus Properties and Radiative Forcing, *J. Geophys. Res.*, 127, e2022JD036 677, <https://doi.org/10.1029/2022JD036677>, 2022.
- Gruber, S., Unterstrasser, S., Bechtold, J., Vogel, H., Jung, M., Pak, H., and Vogel, B.: Contrails and their impact on shortwave radiation and photovoltaic power production – a regional model study, *Atmos. Chem. Phys.*, 18, 6393–6411, <https://doi.org/10.5194/acp-18-6393-2018>,  
100 2018.
- Holzäpfel, F., Gerz, T., and Baumann, R.: The turbulent decay of trailing vortex pairs in stably stratified environments, *Aerosp. Sci. Technol.*, 5, 95–108, 2001.
- Sölch, I. and Kärcher, B.: A large-eddy model for cirrus clouds with explicit aerosol and ice microphysics and Lagrangian ice particle tracking, *Q. J. R. Meteorol. Soc.*, 136, 2074–2093, <https://doi.org/10.1002/qj.689>, 2010.
- 105 Unterstrasser, S.: Properties of young contrails - a parametrisation based on large-eddy simulations, *Atmos. Chem. Phys.*, 16, 2059–2082, <https://doi.org/10.5194/acp-16-2059-2016>, 2016.

Nr	$\hat{f}_{N,s}$	$\tilde{f}_{N,s}$	$z_{\text{atm}}$	$\tilde{z}_{\text{atm}} / \text{m}$	$z_{\text{emit}} / \text{m}$	$\tilde{z}_{\text{emit}} / \text{m}$
1,2,3,4,5	0.06, 0.23, 0.6, 0.87, 0.97	0.05, 0.21, 0.59, 0.87, 0.98	164	163	249	250
6,7,8,9,10	0.0, 0.06, 0.22, 0.58, 0.86	0.0, 0.05, 0.22, 0.59, 0.87	85	87	249	250
11,12,13,14,15,16	0.05, 0.2, 0.57, 0.85, 0.96, 1.0	0.05, 0.19, 0.55, 0.86, 0.97, 1.0	164	163	546	541
17,18,19,20,21	0.08, 0.29, 0.68, 0.9, 0.98	0.08, 0.28, 0.68, 0.91, 0.99	85	87	546	541
22,23,24	0.06, 0.6, 0.97	0.05, 0.59, 0.98	164	163	249	250
25,26,27	0.06, 0.6, 0.97	0.05, 0.59, 0.98	164	163	249	250
28,29,30	0.0, 0.21, 0.86	0.0, 0.21, 0.87	85	87	249	250
31,32,33	0.0, 0.22, 0.86	0.0, 0.22, 0.87	85	87	249	250
34,35,36	0.2, 0.85, 1.0	0.19, 0.85, 1.0	164	163	546	541
37,38,39	0.2, 0.85, 1.0	0.19, 0.86, 1.0	164	163	546	541
40,41,42	0.08, 0.68, 0.98	0.08, 0.68, 0.99	85	87	546	541
43,44,45	0.08, 0.68, 0.98	0.08, 0.68, 0.99	85	87	546	541
46,47,48	0.0, 0.26, 0.94	0.0, 0.25, 0.95	164	163	249	250
49,50,51	0.0, 0.02, 0.73	0.0, 0.02, 0.74	85	87	249	250
52,53,54	0.02, 0.71, 1.0	0.01, 0.7, 1.0	164	163	546	541
55,56,57	0.0, 0.36, 0.96	0.0, 0.35, 0.97	85	87	546	541
Simulations at higher ambient temperatures						
58,59,60,61,62	0.03, 0.14, 0.44, 0.79, 0.94	0.02, 0.13, 0.43, 0.8, 0.95	177	176	110	112
63,64,65,66,67	0.0, 0.01, 0.09, 0.3, 0.69	0.0, 0.0, 0.09, 0.31, 0.7	92	95	110	112
68,69,70,71,72	0.08, 0.28, 0.67, 0.9, 0.98	0.07, 0.27, 0.67, 0.9, 0.99	177	176	262	263
73,74,75,76,77	0.0, 0.07, 0.27, 0.65, 0.89	0.0, 0.07, 0.27, 0.66, 0.9	92	95	262	263
78,79,80,81,82	0.05, 0.21, 0.57, 0.86, 0.97	0.05, 0.2, 0.56, 0.86, 0.97	186	185	163	163
83,84,85,86,87	0.0, 0.03, 0.15, 0.46, 0.81	0.0, 0.03, 0.15, 0.47, 0.82	97	99	163	163
88,89,90,91,92	0.05, 0.19, 0.53, 0.84, 0.96	0.04, 0.17, 0.52, 0.84, 0.96	191	191	123	121
93,94,95,96,97	0.0, 0.02, 0.12, 0.38, 0.76	0.0, 0.02, 0.12, 0.39, 0.77	99	102	123	121
98,99,100	0.04, 0.53, 0.96	0.04, 0.52, 0.96	191	191	123	121
101,102,103	0.05, 0.53, 0.96	0.04, 0.52, 0.97	191	191	123	121
104,105,106	0.0, 0.12, 0.76	0.0, 0.12, 0.77	99	102	123	121
107,108,109	0.0, 0.12, 0.76	0.0, 0.12, 0.77	99	102	123	121
110,111,112,113,114	0.04, 0.18, 0.52, 0.83, 0.96	0.04, 0.16, 0.5, 0.83, 0.96	195	194	102	99
115,116,117,118,119	0.0, 0.01, 0.1, 0.34, 0.73	0.0, 0.01, 0.1, 0.35, 0.74	101	104	102	99
Simulations with A320/B737-like aircraft						
120	0.72	0.72	164	163	176	183
121,122,123	0.13, 0.64, 0.96	0.12, 0.64, 0.97	177	176	76	79
124,125,126	0.03, 0.21, 0.78	0.03, 0.21, 0.8	92	95	76	79
127,128,129	0.2, 0.76, 0.99	0.19, 0.76, 0.99	177	176	185	186
130,131,132	0.07, 0.39, 0.9	0.06, 0.4, 0.91	92	95	185	186
133,134,135	0.17, 0.72, 0.98	0.16, 0.72, 0.98	186	185	114	113
136,137,138	0.04, 0.29, 0.85	0.04, 0.29, 0.86	186	185	114	113
139,140,141	0.16, 0.71, 0.97	0.15, 0.7, 0.98	191	191	85	83
142,143,144	0.04, 0.26, 0.82	0.03, 0.26, 0.83	99	102	85	83
145,146,147	0.16, 0.7, 0.97	0.15, 0.69, 0.98	195	194	70	67
148,149,150	0.03, 0.24, 0.81	0.03, 0.24, 0.82	101	104	70	67

**Table S1.** List of parametrized survival fractions derived with length scales that are computed via the numerical (Eqs. (6) and (7)) or the analytical method (Eqs. (A2) and (A3)), denoted with a tilde, and the corresponding length scales. Rows with three, five, or six simulations correspond to sets where the  $N_0$ -scaling factors 100, 1, 0.01; 100, 10, 1, 0.1, 0.01; or 1000, 100, 10, 1, 0.1, 0.01 are applied, respectively.